2024 IEEE International Conference on Robotics and Automation (ICRA 2024)
May 13-17, 2024. Yokohama, Japan

3D Navigation of a Magnetic Swimmer Using a 2D Ultrasonography Probe Manipulated by a Robotic Arm for Position Feedback

Premal Gorroochurn[1†], Charles P. Hong[2†], Carter M. Klebuc[3†], Yitong Lu[3†], Khue Phan[4†], Javier Garcia[3], Aaron T. Becker[3], and Julien Leclerc[3*]

***Abstract*— Millimeter-scale magnetic rotating swimmers have multiple potential medical applications. They could, for example, navigate inside the bloodstream of a patient toward an occlusion and remove it. Magnetic rotating swimmers have internal magnets and propeller fins with a helical shape. A rotating magnetic field applies torque on the swimmer and makes it rotate. The shape of the swimmer, combined with the rotational movement, generates a propulsive force. Visual feedback is suitable for in-vitro closed-loop control. However, in-vivo procedures will require different feedback modalities due to the opacity of the human body. In this paper, we provide new methods and tools that enable the 3D control of a magnetic swimmer using a 2D ultrasonography device attached to a robotic arm to sense the swimmer's position. We also provide an algorithm that computes the placement of the robotic arm and a controller that keeps the swimmer within the ultrasound imaging slice. The position measurement and closed-loop control were tested experimentally.**

I. Introduction

Minimally Invasive Surgeries (MISs) became widespread in the late 1980s, and their use has steadily increased since then [1], [2]. In 1997, MISs represented 8.9 % of all surgical procedures. This number increased to 11.2 % in 2018 [3]. MISs use smaller incisions and cause less damage to the body than open surgeries. As a result, the risk of infection is reduced, which improves patient outcomes. Patients also recover faster with MISs, and their comfort is improved [4].

Some MISs, such as cardiac catheterization or catheter-directed thrombolysis, are performed using a catheter, which is a thin, flexible tube inserted in the vasculature of a patient [5], [6]. The catheter can be steered to an area to treat and perform a surgical task. Some catheters have tools at their extremity, such as an inflatable balloon, to perform the surgical task [7]. However, the tethered nature of the tool used in these procedures imposes limitations. The precision of the manipulation is limited by the friction between the catheter and the wall of the blood vessel [8]. Catheters rub against the wall of the vessel and can dislodge plaques [9]. Endothelial vascular injury can occur at the catheter insertion site, along the route of the catheter if it rubs or the catheter tip impinges on the vessel wall [10].

This work was supported by the National Science Foundation under Grant Nos. [CPS-1932572, IIS-2130793].

[1]Mechanical Engineering, Columbia University, New York, NY, USA
[2]Biomedical Engineering, Georgia Tech, Atlanta, GA, USA
[3]Electrical and Computer Engineering, University of Houston, TX, USA
[4]Kerr High School, Houston, TX 77083, USA
† Equal contribution, alphabetical order
* Corresponding author. Email: jleclerc@central.uh.edu

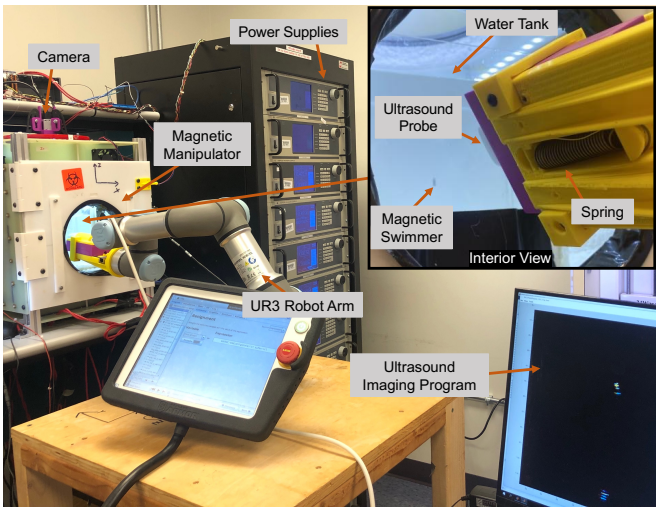

Fig. 1. Experiment setup with the robot arm, power supplies, magnetic manipulator, and a computer running ultrasound imaging program. The inset shows an ultrasound probe and a water tank with a swimmer inside.

Magnetic tetherless robotic agents could be the next step in the evolution of MISs [11]–[14]. Magnetic manipulation controls the position of a magnetic swimmer inside an environment via a magnetic field changing in strength and orientation over time. The properties of the magnetic field are controlled by a robotic system. The magnetic field generated by the magnetic manipulator is at a low frequency (less than 100 Hz), which allows it to pass through the human body. The properties of the magnetic field, coupled with the small nature of the swimmers, allow them to perform MISs. Previous research demonstrated these magnetic robots can be controlled in a simulated physiological environment and perform tasks, such as delivering targeted therapy and clearing blood clots [15].

Our research concentrates on the Magnetic Rotating Swimmer (MRS), a type of magnetic tetherless robotic agent. We target the treatment of pulmonary embolism because pulmonary arteries are deep in the body and difficult to reach using conventional catheters. Our magnetic swimmer is propelled and steered by a magnetic manipulator. A cylindrical magnet with radial magnetization is glued inside the swimmer. The magnetic manipulator creates a magnetic field that generates a torque on the swimmer, making it rotate. Propeller fins on the swimmer convert this rotation into a propulsive force. The magnetic manipulator can steer the swimmers in 3D because they automatically orient themselves with the axis of rotation of the magnetic

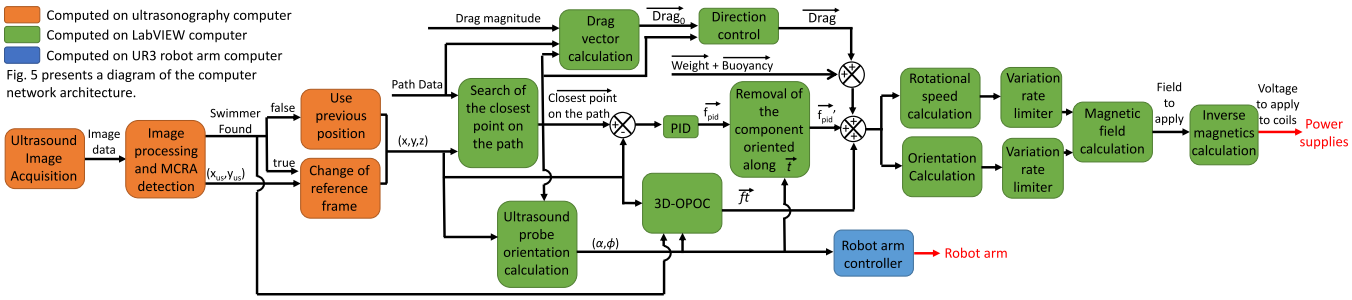

Fig. 2. Functional block diagram of the closed-loop system presented in this paper. Red arrows correspond to the outputs of this diagram.

field. Changing the direction of the magnetic field's rotation axis changes the swimmer's direction.

Navigation of MRS inside small vessels does not require closed-loop control of the radial position of the swimmer. Many previous works steer MRS in a vascular system that constrains the swimmer from moving in a local 1D system [16]–[19]. Previous works have also experimentally demonstrated the control of MRS under ultrasound guidance in restricted channels [20], [21]. If the diameter of the blood vessel is smaller than the length of the MRS, the wall of the arteries guides the swimmer. However, using this method in large vessels, such as the vena cava, which has a diameter of up to 20 mm [22], would likely result in erratic motion of the agent because of wall collisions and unrestricted rotation during these collisions. Closed-loop control of the radial position of MRS inside vessels would allow avoiding collisions with the walls of the arteries and prevent potential damage to the endothelium.

Closed-loop position control of an MRS requires position measurements. Several medical imaging methods are available. X-rays can provide high-resolution images and 3D volume reconstructions with CT scanners. However, X-rays are a form of ionizing radiation, sufficient exposure to which increases the risk of cancer. CT scanners, for example, increase the risk of cancers, and the risk increase is positively correlated with the radiation dose [23]. Excessive exposure to X-rays by the patient would defeat the main purpose of MISs, which is to improve the outcome compared to other surgeries. MRI is another medical imaging method without the drawback of ionizing radiation. However, it uses a strong magnetic field that interacts with the MRS and prevents it from rotating. Photoacoustic imaging is yet another non-ionizing imaging method. It relies on a pulsed laser that locally heats up tissue to produce a thermoelastic expansion and ultrasound wave. These waves are detected and processed to produce an image. This method is sensitive to metallic objects [24], such as the permanent magnets embedded in MRSs. It however suffers from a lower penetration depth than traditional ultrasonography [25] which can also obtain images of an MRS inside a vascular environment [26]. While other groups have demonstrated closed-loop control with X-ray imaging [27], ultrasound can provide position information without dangerous radiation. 3D ultrasonography suffers from a low frame rate, but 2D ultrasonography can provide images at relatively high frequencies. In this paper, we take advantage of the high frame rate and non-ionizing properties of 2D ultrasonography and use this method to obtain position feedback of an MRS.

In the present study, we steered the MRS in an unconstrained cuboid volume to model control in areas where the MRS is small compared to the local physiological environment. This type of steering requires closed-loop control. Our previous work [28] presented a method that allowed closed-loop control of an MRS in 2.5D using a non-moving 2D ultrasonography device for position feedback, which allowed the MRS to follow a horizontal 2D path. Though the off-plane 3D position was unobservable, our control algorithm attempted to steer the MRS back into the imaging slice. Locating and tracking the swimmer in 3D requires coordinated control of the probe's position and orientation. We added software and hardware components to the system and augmented algorithms to enable closed-loop 3D path following by moving an ultrasound probe with a 6-DOF robotic arm.

The chief contribution of this paper is a new closed-loop control method able to steer a free-swimming MRS along an arbitrary 3D path using only data from a 2D ultrasonography device for position feedback. New software modules are introduced: a 3D off-plane oscillation controller (Section III-E), a module that calculates the proper orientation of the ultrasound probe (Section III-A), and a module that performs a change of reference frame from coordinates within the ultrasound imaging slice to the workspace frame (Section III-D). A spring-loaded probe-holding mechanism was also added to the system (Section IV-C).

II. System Overview

The system presented in this paper is a multi-component robotic device augmented from the system presented in [28], [29]. Figure 1 presents pictures of the system.

Figure 2 shows a system functional block diagram. The first step of the algorithm loop is to acquire an ultrasound image, which is then filtered. If the swimmer is detected, the swimmer's position inside the image is calculated. A change of reference frame function is then applied to express the swimmer's position in a reference frame associated with the workspace. This calculation requires the knowledge of the position of the robotic arm, which was calculated in the previous program loop iteration. If the swimmer is not detected, the previous position is used. The closest point on

the path to follow is then searched, and a force component to apply to the swimmer to steer it toward the path centerline is computed from a PID controller. The PID controller only controls the MRS along the r and s axes, which are parallel to the ultrasonography imaging slice (see Fig. 3). Control over the t axis, which is perpendicular to the imaging slice, is performed by a 3D Off Plane Oscillations Controller (3D-OPOC). This module calculates a force $\vec{F_t}$ to apply to the swimmer to keep it inside the imaging slice.

The force magnitude needed to compensate for the drag produced by the swimmer's movement along the trajectory is a user-defined constant. It controls the velocity of the MRS. A module computes the drag vector, which has the same direction as the path centerline at the point closest to the MRS's position. A module changes the direction of the drag vector to make the MRS change direction when it reaches the extremities of the path, which is not closed.

The forces to apply are then summed, and the result is sent to modules that calculate the magnetic field and electromagnet currents to apply. The field and currents calculation is the same as the method presented in [29]. The variation rate of the magnetic field rotation axis and the swimmer's rotational speed is limited because fast variations cause the swimmer to step out of synchronization with the magnetic field and fall to the workspace bottom.

The new orientation of the ultrasound probe is calculated in each iteration, but this information is only sent to the robotic arm every 0.4 seconds to allow the arm to finish its movement before a new movement is requested.

III. Sensing and Control Method

A. Computation of Ultrasound Probe Placement

The ultrasound probe returns a 2D image representing the acoustic return of a nonzero-thickness imaging slice from the workspace. In this subsection, we calculate the equation of an imaging plane and use that to determine the proper orientation of the probe. We define the *imaging plane* as the plane parallel to the imaging slice (i.e., parallel to the (r, s) plane) and at the middle of the imaging slice's thickness (at $t = 0$, see Fig. 3). The goal is to place the imaging plane on the path point closest to the last known position of the swimmer and parallel to the path to follow at this location.

The 3D path to follow is defined by a set of waypoints. We use a total of 1,000 waypoints for a $90\,\mathrm{mm}$ long trajectory, which corresponds to a resolution of $0.09\,\mathrm{mm}$. To compute the equation of the imaging plane, the program first searches for the waypoint closest to the swimmer's last known position. We call this waypoint $\vec{W_{cl}}$. The program then saves the coordinates of the waypoints just after and just before $\vec{W_{cl}}$. These two points are called $\vec{P_1}$ and $\vec{P_2}$ and lie in the desired imaging plane. Three points are needed to define a plane. We chose to use the position of the tip of the ultrasound probe as the third point. We are free to choose the position on this point. We chose to keep the probe on the wall of our workspace at $x = z = 0$. The coordinates of the third point P_3 of the imaging plane are therefore $(0, -L_w/2, 0)$ in the (x, y, z) coordinate system where L_w is the length of the workspace in the y direction.

The general equation of a plane is

$$a \cdot x + b \cdot y + c \cdot z + d = 0\,. \tag{1}$$

Vector $\vec{P_0} = \begin{bmatrix} a & b & c \end{bmatrix}^\top$ is perpendicular to the imaging plane. Constants a, b, and c are calculated as

$$\begin{bmatrix} a & b & c \end{bmatrix}^\top = \vec{P_0} = (\vec{P_3} - \vec{P_1}) \times (\vec{P_3} - \vec{P_2})\,. \tag{2}$$

The constant d can be calculated with $d = b \cdot L_w/2$.

The z positions z_1 and z_2 of the plane at the intersections with the edges of the front side of the workspace are then calculated with the following equations:

$$z_1 = (+a \cdot L_w + b \cdot L_w - d)/c \tag{3}$$

$$z_2 = (-a \cdot L_w + b \cdot L_w - d)/c \tag{4}$$

The rotation angle of the plane around axis x is

$$\phi = -\operatorname{atan2}(z_2 - z_1, L_w)\,. \tag{5}$$

The rotation angle of the plane around axis y is

$$\alpha = -\operatorname{atan2}(c, a)\,. \tag{6}$$

B. Swimmer Detection in Ultrasonography Images

Previous work [28] found that Doppler mode ultrasonography led to better swimmer localization results than B-mode. The liquid flowing around the swimmer generates a strong Doppler signal that can be used in detection algorithms. Swimmer detection is done via an intensity-based algorithm focused on finding the brightest pixel after applying a 5-by-5-pixel median filter to the Doppler mode image.

C. Ultrasound Calibration

A 3D-printed checkerboard skeleton was used to calibrate the ultrasound images. This board consists of squares with diagonals of $20\,\mathrm{mm}$ and was placed inside a water tank in the center of the magnetic manipulator. Ultrasound B-mode images of the skeleton were recorded, revealing the rib intersections. Images were processed to determine the physical pixel size along the r and s axes. The conversion factor c_s for the s axis is $0.295\,\mathrm{mm}$/pixel with a relative error of $4\,\%$. In the r axis, conversion factor c_r is $0.265\,\mathrm{mm}$/pixel with a relative error of $0.8\,\%$. These factors are used to convert pixel coordinates into millimeter coordinates in Section III-D.

D. Change of Reference Frame

The swimmer's location within the ultrasound image frame $[s, r, 0]$ must be converted to a set of coordinates in the reference frame of the workspace $[x, y, z]$. The raw ultrasound image is 400×386 pixels. The origin of the raw ultrasound image is in the top-left corner. The following equations center the reference frame at $s = 0$ and convert pixel coordinates (r_{px}, s_{px}) into millimeter coordinates:

$$s = (s_{px} - 386/2) \times c_s\,, \tag{7}$$

$$r = r_{px} \times c_r\,, \tag{8}$$

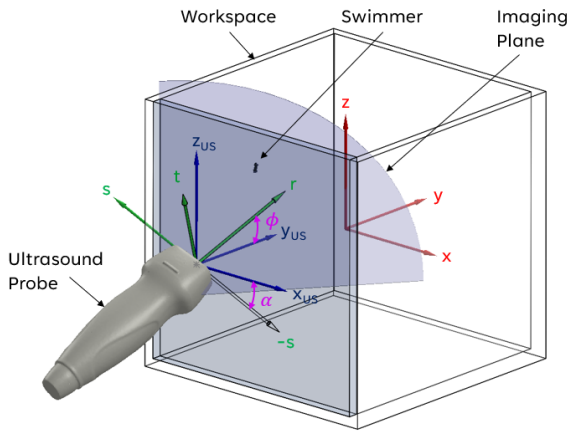

Fig. 3. 3D CAD representation of coordinate transformations between ultrasound reference frame (green) and workspace reference frame (red). The ultrasound probe only detects the swimmer on its imaging plane (purple); thus, the MRS's position when detected in the ultrasound image will always be at $t = 0$. An intermediate coordinate system (blue) is used to assist the transformation between the two frames. The angles ϕ and α are shown in pink. The s-direction must be inverted before coordinate transformations can be applied.

Next, rotation matrices are used to convert the coordinates r and s into the workspace reference frame:

$$R_{y,\alpha} = \begin{bmatrix} \cos(\alpha) & 0 & \sin(\alpha) \\ 0 & 1 & 0 \\ -\sin(\alpha) & 0 & \cos(\alpha) \end{bmatrix}, \; R_{x,\phi} = \begin{bmatrix} 1 & 0 & 0 \\ 0 & \cos(\phi) & -\sin(\phi) \\ 0 & \sin(\phi) & \cos(\phi) \end{bmatrix} \quad (9)$$

The swimmer position $\overrightarrow{p_r}$ in the workspace frame is

$$\overrightarrow{p_r} = R_{y,\alpha} R_{x,\phi} \cdot [-s, r, 0]^\top + \overrightarrow{p}_{usp}\,, \quad (10)$$

where $\overrightarrow{p}_{usp}$ is the position of the ultrasound probe tip expressed in the workspace reference frame.

E. 3D Off Plane Oscillation Controller

The previous paper [28] introduced an *Off Plane Oscillation Controller* (OPOC) that allows keeping the swimmer inside the 2D ultrasonography imaging plane. In this previous publication, the robotic arm holding the ultrasound probe was not moving, and the reference frame (r, s, t) associated with the probe was parallel to the reference frame (x, y, z) associated with the workspace. The direction of the swimmer was controlled in 3D, and the swimmer followed a 2D path coplanar to the x-y plane. In the present paper, we modified the OPOC to allow the swimmer to follow a 3D path. To differentiate it from the previous version, we call this controller 3D-OPOC.

In our previous paper, a force $\vec{F}_t$ was applied by the OPOC to the magnetic swimmer in addition to the forces calculated by other controllers. This additional force changes direction when the swimmer disappears from the ultrasonography image, making the swimmer oscillate within and around the imaging slice. In that study, $\vec{F}_t$ was always oriented vertically because the ultrasound probe did not change orientation.

With the 3D-OPOC, a force $\vec{F}_t$ is still present but is oriented perpendicular to the imaging plane. The rotation matrices in Eqns. (9) are used to calculate $\vec{F}_t$ (see Alg. 1).

Algorithm 1: CALCULATION OF $\vec{F}_t$

```
F⃗_t0 ← [0, 0, f_t0]^⊤ ; // force F⃗_t before rotation.
n ← 2 ; // filter length: number of failed detections needed to reverse direction.
nNotFound ← n ; // initialize a variable to store the number of times steps since the last swimmer detection.
k ← 1 ; // Initial direction of F⃗_t. The swimmer needs to start with a force pointing upward to cross the US beam.
Loop
    SwimmerFound ← USDETECTION() ;
    // measure using the ultrasonography device. True if the swimmer is detected.
    if SwimmerFound then
        nNotFound ← 0 ;
    else
        nNotFound ← nNotFound +1 ;
        if nNotFound ≡ n then
            k ← −k ; // reverse direction of F⃗_t.
        end
    end
    F⃗_t ← k · R_{y,α} · R_{y,φ} · F⃗_t0 ; // force vector to apply calculation.
EndLoop
```

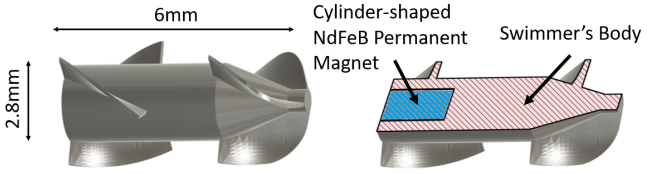

Fig. 4. 3D CAD representation of swimmer with internal NdFeB magnet.

IV. EXPERIMENTAL SETUP

A. Electromagnetic Actuation

The magnetic manipulator consists of six electromagnets oriented in a cube shape and separated by 300 mm. Each electromagnet has an internal diameter of 180 mm and an external diameter of 220 mm. Each electromagnet is powered by two Kepco BOP 20-50MG power supplies connected in series. A National Instruments IC3173 industrial controller generates an analog signal to control the power supplies. Two Basler acA800 cameras are mounted on the top and right side of the magnetic manipulator to measure the swimmer's position during path-following.

B. Design and Fabrication of the Swimmers

The magnetic rotating swimmer in this experiment has three head helices and three body helices (see Fig. 4). The bottom pitch of the helices is 16 mm, and the top pitch is 12 mm. The swimmer diameter is 2.8 mm and the length is 6 mm. These dimensions ensure the swimmer is small enough to be inserted inside a vessel yet large enough to be efficiently manufactured.

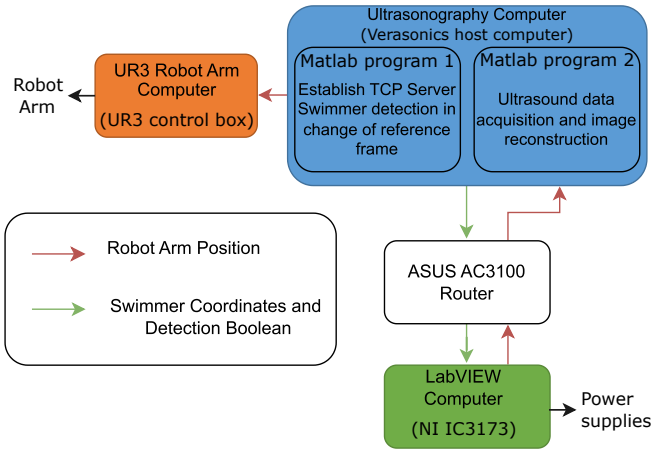

Fig. 5. Block diagram of the computer network transferring ultrasound and robot arm data.

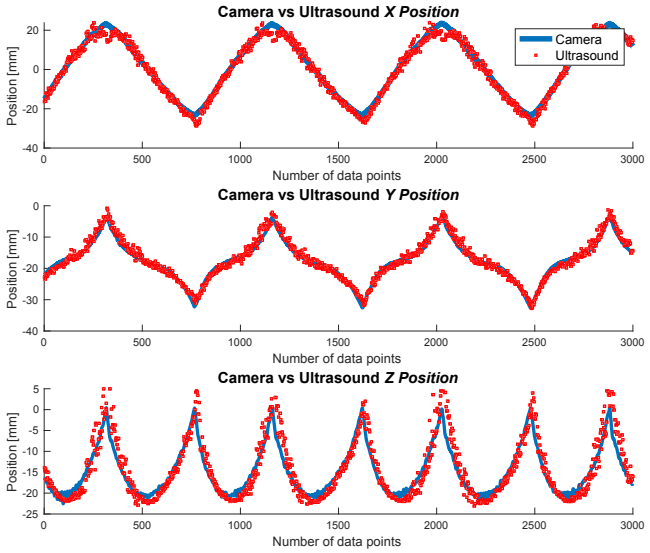

Fig. 6. Plot of swimmer's positions measured with cameras and ultrasound using camera feedback (3000 points are shown for a 60 s experiment).

Figure 4 shows the design of the swimmer used in this paper. The swimmer is printed using a Formlabs resin 3D printer. Then, the swimmer is washed using ethanol inside an ANYCUBIC wash and cure station for around 6 minutes. After washing, the swimmer is placed under a UV light for 20 minutes to cure the resin and strengthen the design. One cylinder-shaped NdFeB permanent magnet (1 mm diameter, 1.5 mm length) is placed inside the swimmer. A small amount of epoxy is added at the bottom of the swimmer and ensures that the magnet stays in place.

C. Ultrasonography Hardware

The ultrasound system utilized in this experiment is a Verasonics Vantage 32 LE with a 64-element 1D phased array transducer. A configuration file in the form of a MATLAB script is used to set the parameters of the ultrasound acquisition. The frequency of the ultrasound probe is 3 MHz. The configured threshold of the Doppler signal is 0.2 (20 %).

The ultrasound system is connected to a host controller computer. The control and data acquisition of the ultrasound transducer is controlled via a MATLAB graphical user interface (GUI). An ultrasound gel pad (diameter 90 mm, thickness 20 mm) is placed between the probe and the wall of the water tank to reduce the acoustic impedance at this interface. Furthermore, as the probe is rotated, the extremities of the probe tip may be pushed against the gel pad, and so a spring-loaded probe holder is used to allow the probe to move back to prevent damaging the workspace.

D. Data Transfer Between Computers

The Verasonics Host Computer is connected to a National Instrument IC3173 through a TCP/IP connection via an ASUS AC3100 Router (see Fig. 5). The Verasonics computer sends the MRS position to the IC3173 using this connection. A LabVIEW script in the IC3173 calculates the pose for the UR3 robot arm. The generated pose is sent via the Verasonics computer to the UR3 arm.

E. Robot Arm Program

A program moving the robotic arm is implemented on the UR3 robot arm computer. The program is a combination of its visual scripting language and URscript commands. On startup, a connection is established to the Verasonics host computer hosting the TCP server. The robot arm waits for a set of arm pose coordinates sent as a string variable. Robot arm pose coordinates are composed of linear translation values (in millimeters) and rotational values (in radians) along the x, y, and z axes. Each set of coordinates is enclosed with "<" and ">" symbols. These symbols allow the program to distinguish between multiple sets of coordinates. Individual coordinates are extracted from the string and placed into variables. The linear translation coordinates are converted from meters to millimeters. A pose variable is generated, and the robot arm moves to this specified pose in a timeframe of 400 ms. The `moveL` function inside the URScript program moves the arm to the correct position.

V. Experimental Results

A. Swimmer Position Measurement Using Ultrasonography

We first validated the proposed swimmer position measurement method by making the swimmer follow a predefined 3D path in a water tank using camera feedback to close the control loop. The ultrasound transducer was attached to the robotic arm, which set the pose of the transducer. The probe orientation was calculated using the method presented in Section III-A. The position in the workspace reference frame was calculated using the method introduced in Section III-D. We compared the position information measured using cameras and ultrasound. An offset was manually tuned on the LabVIEW interface to align the ultrasonography and camera position measurements. The path to follow was designed as a twisted U-shape. The path is the same shape as the one presented in Fig. 7. The experimental results are shown in Fig. 6. The ultrasound measurements were in good agreement with the measurements using cameras. The RMS error between camera measurements and ultrasound was 3.41 ± 2.48 mm (1.88 ± 1.65 mm about the x axis,

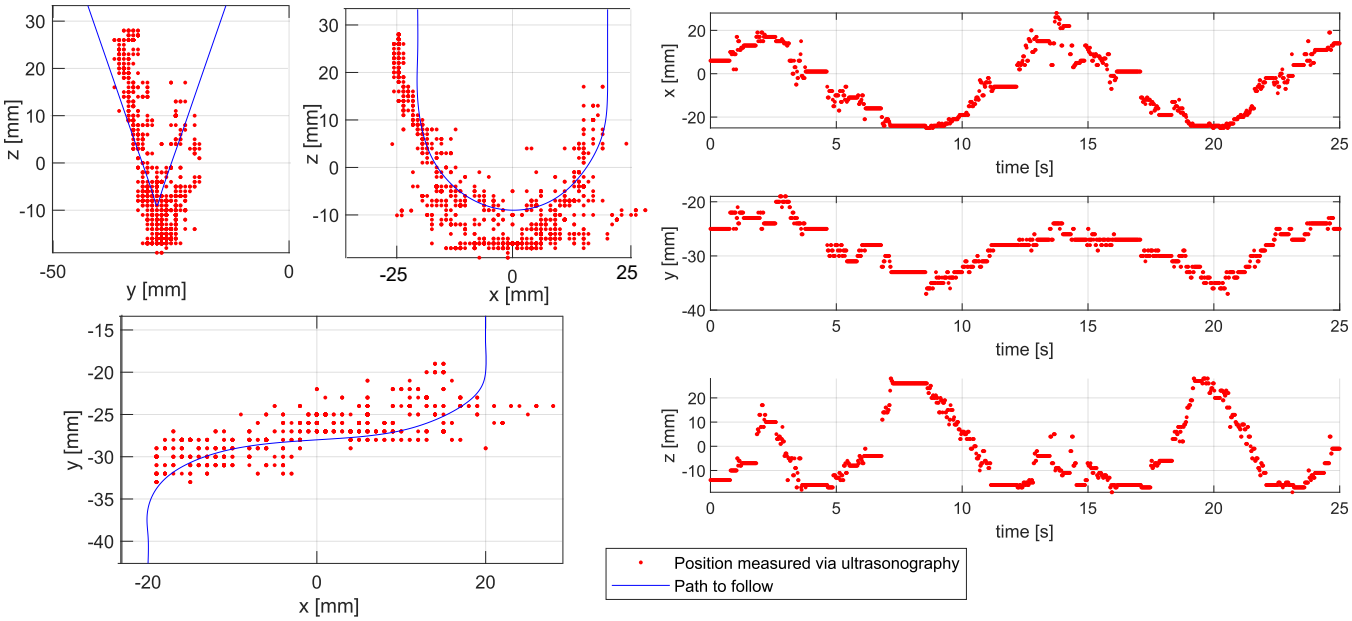

Fig. 7. Experimental results of system presented in Fig. 2. The system was controlled in a closed loop using only ultrasound data.

$1.08 \pm 0.8\,\mathrm{mm}$ about the y axis, and $2.16 \pm 2.25\,\mathrm{mm}$ about the z axis).

B. Closed-loop Control with Ultrasonography Feedback

The system shown in Fig. 2 was configured to follow the 3D path shown in Fig. 7. The swimmer started from the bottom of the workspace. The swimmer first swam vertically upward until it was detected by the ultrasound device. Closed-loop control started automatically after the first detection.

Many tests were performed, and the controller parameters were tuned manually using the test results. An experimental path followed by the swimmer is shown in Fig. 7. The swimmer followed the path centerline with an average distance from the centerline of $5.8\,\mathrm{mm}$. During the tests, the system always lost control of the MRS after it followed the path for a relatively short duration (less than 30 seconds). Though the present state of this control method is insufficient for the full duration of surgery, it could complement an imaging method that uses X-rays. The X-rays could be temporarily activated only if tracking with ultrasonography is lost. This method could significantly reduce patient exposure to X-rays.

VI. Conclusion

This work introduces methods and experimentally demonstrates the 3D closed-loop control of an MRS using only 2D ultrasonography for position feedback. This would enable the swimmer to navigate medically relevant environments, such as the pulmonary artery.

In Section V-A, we show that the position of an MRS can be measured using a 2D ultrasound probe attached to a robotic arm. The swimmer position measured by an optical camera is in good agreement with measurements using ultrasonography. In Section V-B, the system's loop was closed using ultrasonography only for position feedback. The proposed system can stabilize the swimmer for short durations before losing tracking and control. The system is not observable along the t axis of the ultrasound device and, even if the 3D-OPOC can temporarily stabilize the swimmer's position, it eventually fails to keep it stable. While this method cannot be used alone to perform surgical procedures, it could be complemented by an imaging method based on X-rays, which would only be activated temporarily when tracking with ultrasound is lost.

In the future, the system could be remotely controlled by a qualified surgeon. Remote accessibility will enable the MRS to be used in many different communities, including small hospitals where a qualified surgeon is unavailable. The use of ultrasonography, a technology widely available within clinics, paired with the presented control method, will reduce the patient's exposure to X-rays in tracking the swimmer and decrease the risk of cancer.

Modifications will be made to improve the system's precision and accuracy. An improvement involves the utilization of a computer vision algorithm. An object recognition algorithm could allow the system to identify the swimmer even when noise and external factors are present (blood vessel walls, distortion from blood flow, etc.). Additionally, we are considering the use of magnetic sensors, such as Hall-effect sensors, to localize the swimmer based on the magnetic field generated by its magnet, similar to [30].

Another future avenue consists of introducing a geometrically accurate phantom of pulmonary arteries with pulsating flow to more closely reflect the true nature of vascular environments. Finally, further miniaturization of the swimmers can be pursued to allow access to more narrow blood vessels, such as those beyond the first branches of the pulmonary arteries and those in the brain.

REFERENCES

[1] A. S. John, I. Caturegli, N. S. Kubicki, and S. M. Kavic, "The rise of minimally invasive surgery: 16 year analysis of the progressive replacement of open surgery with laparoscopy," *JSLS: Journal of the Society of Laparoscopic & Robotic Surgeons*, vol. 24, no. 4, 2020.

[2] A. G. Harrell and B. T. Heniford, "Minimally invasive abdominal surgery: lux et veritas past, present, and future," *The American journal of surgery*, vol. 190, no. 2, pp. 239–243, 2005.

[3] A. S. Mattingly, M. M. Chen, V. Divi, F. C. Holsinger, and A. Saraswathula, "Minimally invasive surgery in the united states, 2022: Understanding its value using new datasets," *Journal of Surgical Research*, vol. 281, pp. 33–36, 2023.

[4] M. De Prado, M. Cuervas-Mons, and V. De Prado, "Open vs minimally invasive surgery: Advantages and disadvantages," in *Foot and Ankle Disorders: A Comprehensive Approach in Pediatric and Adult Populations*. Springer, 2022, pp. 43–69.

[5] M. J. Kern, P. Sorajja, and M. J. Lim, *Cardiac catheterization handbook*. Elsevier Health Sciences, 2015.

[6] A. E. Lewis, N. S. Gerstein, R. Venkataramani, and H. Ramakrishna, "Evolving management trends and outcomes in catheter management of acute pulmonary embolism," *Journal of Cardiothoracic and Vascular Anesthesia*, vol. 36, no. 8, pp. 3344–3356, 2022.

[7] R. A. Byrne, G. W. Stone, J. Ormiston, and A. Kastrati, "Coronary balloon angioplasty, stents, and scaffolds," *The Lancet*, vol. 390, no. 10096, pp. 781–792, 2017.

[8] K. Takashima, R. Shimomura, T. Kitou, H. Terada, K. Yoshinaka, and K. Ikeuchi, "Contact and friction between catheter and blood vessel," *Tribology International*, vol. 40, no. 2, pp. 319–328, 2007, first International Conference on Advanced Tribology (iCAT 2004). [Online]. Available: https://www.sciencedirect.com/science/article/pii/S0301679X0600123X

[9] H. Eggebrecht, O. Oldenburg, O. Dirsch, M. Haude, D. Baumgart, D. Welge, J. Herrmann, G. Arnold, K. Werner Schmid, and R. Erbel, "Potential embolization by atherosclerotic debris dislodged from aortic wall during cardiac catheterization:: histological and clinical findings in 7,621 patients," *Catheterization and cardiovascular interventions*, vol. 49, no. 4, pp. 389–394, 2000.

[10] N. Nakazawa, "Infectious and thrombotic complications of central venous catheters," in *Seminars in oncology nursing*, vol. 26, no. 2. Elsevier, 2010, pp. 121–131.

[11] Y. Alapan, U. Bozuyuk, P. Erkoc, A. C. Karacakol, and M. Sitti, "Multifunctional surface microrollers for targeted cargo delivery in physiological blood flow," *Science robotics*, vol. 5, no. 42, p. eaba5726, 2020.

[12] Q. Ze, S. Wu, J. Dai, S. Leanza, G. Ikeda, P. C. Yang, G. Iaccarino, and R. R. Zhao, "Spinning-enabled wireless amphibious origami millirobot," *Nature communications*, vol. 13, no. 1, p. 3118, 2022.

[13] T. Wang, H. Ugurlu, Y. Yan, M. Li, M. Li, A.-M. Wild, E. Yildiz, M. Schneider, D. Sheehan, W. Hu *et al.*, "Adaptive wireless millirobotic locomotion into distal vasculature," *Nature communications*, vol. 13, no. 1, p. 4465, 2022.

[14] D. Jin, Q. Wang, K. F. Chan, N. Xia, H. Yang, Q. Wang, S. C. H. Yu, and L. Zhang, "Swarming self-adhesive microgels enabled aneurysm on-demand embolization in physiological blood flow," *Science Advances*, vol. 9, no. 19, p. eadf9278, 2023.

[15] I. S. Khalil, A. Adel, D. Mahdy, M. M. Micheal, M. Mansour, N. Hamdi, and S. Misra, "Magnetic localization and control of helical robots for clearing superficial blood clots," *APL bioengineering*, vol. 3, no. 2, p. 026104, 2019.

[16] H. J. Lee and S. M. Jeon, "An intravascular helical magnetic millirobot with a gripper mechanism performing object delivery and collecting motions actuated by precession rotating magnetic fields," *AIP Advances*, vol. 11, no. 2, p. 025236, 02 2021. [Online]. Available: https://doi.org/10.1063/9.0000006

[17] S. Jeong, H. Choi, K. Cha, J. Li, J.-o. Park, and S. Park, "Enhanced locomotive and drilling microrobot using precessional and gradient magnetic field," *Sensors and Actuators A: Physical*, vol. 171, no. 2, pp. 429–435, 2011.

[18] A. Hosney, J. Abdalla, I. S. Amin, N. Hamdi, and I. S. Khalil, "In vitro validation of clearing clogged vessels using microrobots," in *2016 6th IEEE International Conference on Biomedical Robotics and Biomechatronics (BioRob)*. IEEE, 2016, pp. 272–277.

[19] J. Nam, W. Lee, J. Kim, and G. Jang, "Magnetic helical robot for targeted drug-delivery in tubular environments," *IEEE/ASME Transactions on Mechatronics*, vol. 22, no. 6, pp. 2461–2468, 2017.

[20] Q. Wang, X. Du, D. Jin, and L. Zhang, "Real-time ultrasound doppler tracking and autonomous navigation of a miniature helical robot for accelerating thrombolysis in dynamic blood flow," *ACS nano*, 2022.

[21] X. Du, Q. Wang, D. Jin, P. W. Y. Chiu, C. P. Pang, K. K. L. Chong, and L. Zhang, "Real-time navigation of an untethered miniature robot using mobile ultrasound imaging and magnetic actuation systems," *IEEE Robotics and Automation Letters*, vol. 7, no. 3, pp. 7668–7675, 2022.

[22] A. Malik, M. Chaudhry, M. Abdullah, S. H. Inam, and N. Iqbal, "Idiopathic dilatation of inferior vena cava: A case report," *Cureus*, 2020.

[23] C.-F. Cao, K.-L. Ma, H. Shan, T.-F. Liu, S.-Q. Zhao, Y. Wan, and H.-Q. Wang, " scans and cancer risks: A systematic review and dose-response meta-analysis," *BMC cancer*, vol. 22, no. 1, p. 1238, 2022.

[24] Y. Yan, W. Jing, and M. Mehrmohammadi, "Photoacoustic imaging to track magnetic-manipulated micro-robots in deep tissue," *Sensors*, vol. 20, no. 10, p. 2816, 2020.

[25] S. Liu, T. Wang, X. Zheng, Y. Zhu, and C. Tian, "On the imaging depth limit of photoacoustic tomography in the visible and first near-infrared windows," *Optics Express*, vol. 32, no. 4, pp. 5460–5480, 2024.

[26] T. Maecken and T. Grau, "Ultrasound imaging in vascular access," *Critical Care Medicine*, vol. 35, no. Suppl, p. S178–S185, May 2007.

[27] J. Sa, J. Park, E. Jung, N. Kim, D. Lee, S. Bae, Y. Lee, and G. Jang, "Separable and recombinable magnetic robot for robotic endovascular intervention," *IEEE Robotics and Automation Letters*, vol. 8, no. 4, pp. 1881–1888, April 2023.

[28] Y. Lu, H. Zhao, A. Becker, and L. Julien, "Steering rotating magnetic swimmers in 2.5 dimensions using only 2d ultrasonography for position sensing," *IEEE Robotics and Automation Letters*, 2022.

[29] J. Leclerc, H. Zhao, D. Z. Bao, A. T. Becker, M. Ghosn, and D. J. Shah, "Agile 3d-navigation of a helical magnetic swimmer," in *2020 IEEE International Conference on Robotics and Automation (ICRA)*. IEEE, 2020, pp. 7638–7644.

[30] M. Zhang, L. Yang, C. Zhang, Z. Yang, and L. Zhang, "A 5-d large-workspace magnetic localization and actuation system based on an eye-in-hand magnetic sensor array and mobile coils," *IEEE Transactions on Instrumentation and Measurement*, vol. 72, pp. 1–11, 2023.